Volume 4
Number 11
November 2025
Pages 1315–1404

Energy Advances

rsc.li/energy-advances

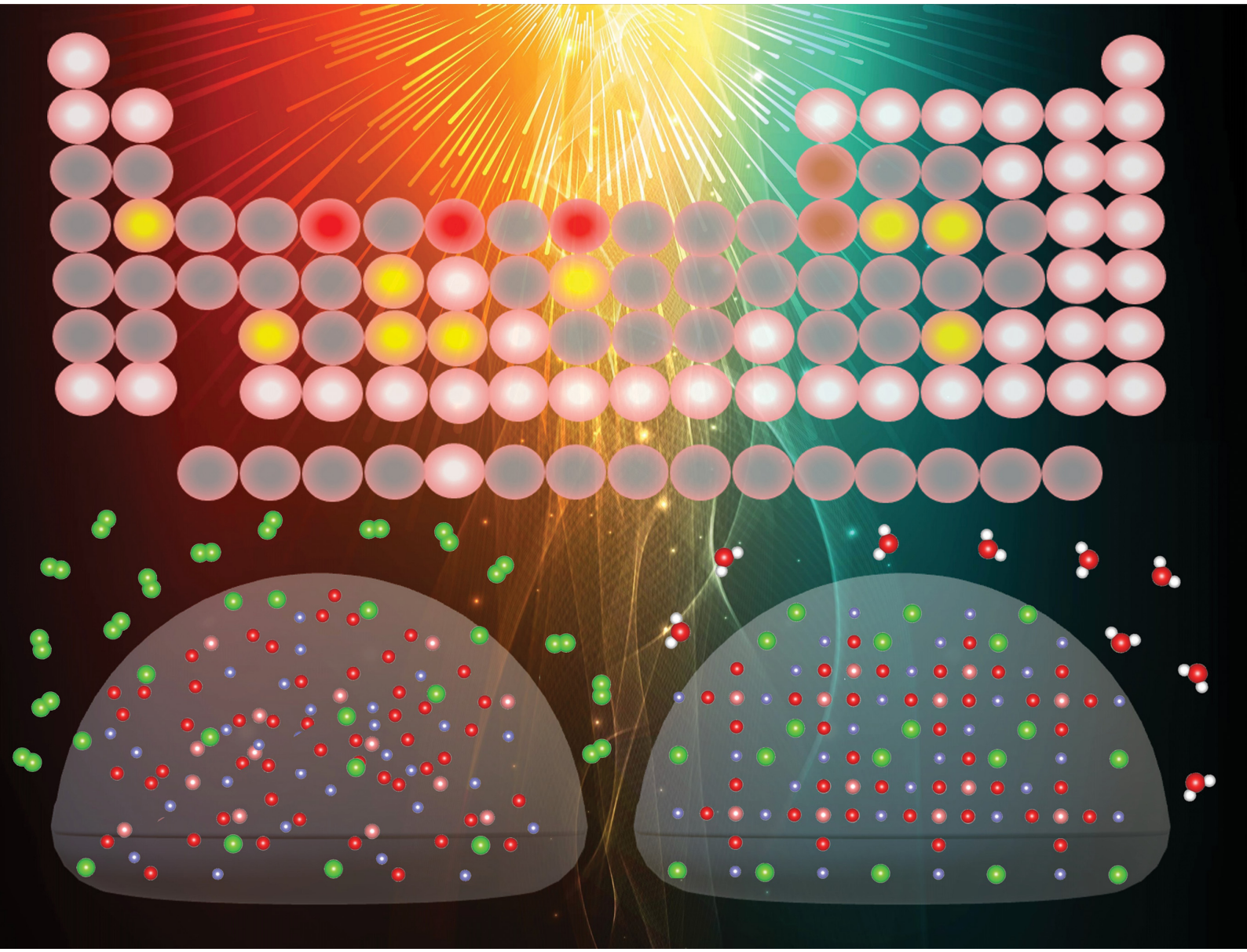

ISSN 2753-1457

ROYAL SOCIETY OF CHEMISTRY

PAPER

Eric McCalla *et al.*

High-throughput methods to design deformable recrystallized boracite solid electrolytes: challenges and solutions

Energy Advances

ROYAL SOCIETY OF CHEMISTRY

PAPER

View Article Online
View Journal | View Issue

Cite this: *Energy Adv.*, 2025, 4, 1337

High-throughput methods to design deformable recrystallized boracite solid electrolytes: challenges and solutions

Jean-Danick Lavertu,[a] Sibyl Martasek,[a] Sara Reardon,[a] Shipeng Jia,[a] Antranik Jonderian,[a] Giyun Kwon,[b] Youngjoon Bae[b] and Eric McCalla *[a]

Solid electrolytes for Li batteries continue to be extremely challenging to design as they have such broad material requirements. No single material matches all required properties. Boracites have recently been studied as being potentially ideal in terms of being deformable in a glassy state so that they can be well prepared in a composite with the cathodes, but then be crystallized into an ionic conductor at temperatures that do not damage the cathodes. However, these materials remain poorly explored, primarily due to the time/effort needed to perform the complex synthesis. Herein, we develop a combinatorial workflow that allows reproduction of materials made previously only in bulk quantities. In so doing, we overcome the extreme Cl loss that leaves no Cl in our small samples when we attempt to utilize the same synthesis conditions published previously for larger samples. The Cl loss is mitigated through saturation of the atmosphere such that equilibrium is established to maintain sufficient Cl content. This establishes atmosphere saturation as a method for mitigating extreme elemental loss in combinatorial samples. We further demonstrate that our materials show comparable ionic conductivity to those published previously. We also determine the limits to the stability window for the first time and also identify air stability as a serious problem for these materials as it converts them into proton conductors. Finally, we demonstrate the viability of thorough dopant screening by testing the deformability of a batch of samples made with 62 different dopants and find the property to be highly tunable with composition. This shows that combinatorial methods will be viable and highly efficient in developing these promising materials.

Received 4th July 2025,
Accepted 5th October 2025

DOI: 10.1039/d5ya00188a

rsc.li/energy-advances

1. Introduction

Lithium-ion batteries (LIBs) have established themselves as the standard for rechargeable batteries across multiple fields. Their energy density, long life and safety has cemented their use in everyday life.[1] Despite the success of these batteries, there are continued safety concerns related to the use of flammable organic liquid electrolytes. These are prone to thermal runaway and even catching fire[2] and formation of Li dendrites prevents the use of Li as the anode, thereby setting a limit on the energy density of the battery.[3] Electrolytes ensure the efficient travel of Li ions between the cathode and anode, and although typical carbonate-based electrolytes like LP30 benefit from high lithium conductivity, they are flammable, undergo side reactions during battery cycling and do not prevent the formation of dendrites within the battery.[4]

Solid electrolytes have emerged as an attractive solution to liquid electrolyte because of their superior safety, stability and potential for higher energy density by preventing Li dendrites and thereby enabling the use of Li metal as the anode.[5] Solid electrolytes do have shortcomings, as they tend to have lower lithium conductivity compared to commercial liquid electrolytes. However, this short-coming has been overcome in recent years with the advent of highly conductive solid–electrolytes such as some sulfides.[6] Despite this success, all-solid batteries have not been commercialized, in large part due to problems at the interfaces between the solid electrolytes and both electrodes. Large interfacial resistance can be debilitating with some solid electrolytes such as the garnet oxides.[6] In other more deformable materials, such as the sulfides, the interfacial resistance is not an issue, but the electrolyte is electrochemically unstable at both high voltage where relevant cathodes operate and at low potentials where anodes operate.[6]

The daunting challenge of designing a viable solid electrolyte therefore lies in needing to optimize several properties: (1) high ionic conductivity, (2) low electronic conductivity, (3) electrochemical and chemical stability at both high and low voltage, and (4) low contact resistance between itself and both the cathode and anode materials. We have recently designed a suite of high-throughput measurements that allows for the

[a] *McGill University, Montreal, Quebec, Canada. E-mail: eric.mccalla@mcgill.ca*
[b] *Battery Material Technical Unit, Samsung Advanced Institute of Technology, Samsung Electronics, Suwon, Gyeonggi-do, 16678, Republic of Korea*

quantification of each of these metrics (except the contact resistance).[7] We have further developed a synthesis route to prepare glassy electrolytes, and further developed a high-throughput test to quantify the deformability of the electrolyte at temperatures where solid batteries are normally processed.[8] This deformability serves as a proxy for contact resistance, as it is certainly a necessary condition to get good mixing between the electrode and electrolyte and thus obtain decreased contact resistance. The established workflow allows for the preparation and characterization of samples in batches of 64 without any bottleneck.[9]

We have used this workflow to optimize electrolyte properties in borosilicate materials by melt-quenching them from 900 °C. Though we were able to dramatically improve deformability in the borosilicates, we find limited potential to increase their ionic conductivity.[8] However, numerous other classes of glassy solid electrolytes exist.[10–12] One family of materials that shows an interesting combination of properties is the boracites with composition $Li_4B_{7-x}M_xO_{12}X$ where M is an element introduced to improve the ionic conductivity and X is a halogen.[13–17] Previous studies mostly focussed on M = Al and Ga only and obtained ionic conductivities up to 10^{-5} S cm^{-1}.[18,19] Recent studies have also doped the material by partial replacement of the Li by Mg, also increasing the conductivity to 10^{-5} S cm^{-1}.[20] Interestingly, the materials can first be prepared as a glass by quenching between 1000 °C and 1300 °C and then they can be crystallized into the boracite phase by heating to moderate temperatures as low as 500 °C. This offers unique prospects wherein the more deformable glassy material can be mixed with the cathode material and then processed into the crystalline form during battery manufacture. However, ionic conductivity remains the only relevant electrolyte property that has been measured for these materials, and the composition spaces remains woefully underexplored.

Herein, we adapt our high-throughput approach used on the borosilicates for use with the boracites. Importantly, this meant mitigating the extreme chlorine loss that occurs in these materials, an issue that is rarely discussed in the literature. We further characterize the materials, not only for ionic conductivity but we also determine the electrochemical stability window for the first time as well as the ionic conductivity. We also identify moisture instability as a serious concern in this class of material, particularly when excess Cl is present in the material, possibly as amorphous LiCl. Finally, we demonstrate the potential of the high-throughput approach by preparing glassy materials with 62 different dopants and finding dramatic impact on the deformability. This work will guide further design of this intriguing class of solid electrolytes.

2. Experimental methods

2.1 Glass/ceramic preparation

Lithium chloride (~2 M in water), boric acid (~2 M in methanol), gallium nitrate (~1.5 M in water) were dispensed with the molar ratio $LiCl/(H_3BO_3 + Ga(NO_3)_3) = 0.71$ for Ga-doped samples and a total of 3.4 mmol. Any dopant (if applicable) was also dispensed at this time. The borosilicate glass vials containing the samples were then heated at 75 °C overnight. The vials were then taken to a furnace where they were calcined at 500 °C (heated from room temperature in around 30 minutes) for up to an hour. The temperature was held at 200 °C and 300 °C for a few minutes when the residue was not already well dried. Once taken out of the furnace and cooled, the residue was then scraped, crushed and mixed inside the vial. This resulting powder could then be transferred to a high-throughput pellet press where pistons in each well were pressed enough so that a pellet could hold itself together. Once pressed and taken out of the block, the pellets were put on small and shallow platinum cups, on top of a larger platinum sheet. If the pellets were particularly humid, a quick heating step could be done at 500 °C (the pellets may swell) to prevent the pellets from moving in the next step. 32 or 64 pellets at once were slid into a preheated furnace at 950 °C (or higher if needed) to melt them for 10 min, then slid back out to quench them. Alternatively, 8 pellets were covered by a small alumina ceramic boat (or individual pellets under small crucibles) to mitigate chlorine loss, then slid in and out the same way.

2.2 Characterization

After being melted and quenched, the samples can undergo a Brinell hardness test. The deformability of the samples was investigated in high-throughput using a custom designed setup.[8] The glass ceramic samples were lined up 8 by 8 on an alumina plate underneath an elevated steel block with 64 holes aligned with the samples. Zirconia spheres could then be placed on top of the samples and individually weighed down by a bolt with nuts, totaling 24 g. The setup was heated rapidly to 400 °C, then heated to 500 °C over 2 h and held there for an hour. The diameter of the dimple was then measured using a micrometer across the surface. This procedure, colloquially called the ''dimple test'', is known as the Brinell hardness test, which quantifies the hardness of a given material as BHN (Brinell hardness number), defined as $BHN = \frac{2P}{\pi D\left(D - \sqrt{D^2 - d^2}\right)}$, where P is the applied load in kg, D is the diameter of the sphere, and d is the diameter of the indentation left by the sphere. To express the ability of the sample to espouse the sphere, we take the inverse of this number (1/BHN) as the deformability in mm^2 kg^{-1}. To give a sense of scale, carrying out the same test on adhesive putty at room temperature gave a deformability of 100 mm^2 kg^{-1}. We also ensured that the zirconia spheres did not touch the platinum cup.

After obtaining the BHN, the samples could then be crystallized, by heating to 525 °C for 3 hours, rushed to the glovebox, then polished with a sanding strip (enough to reach the indentation).

To carry out the conductivity measurements, the samples were covered with a mask with circular holes aligned with the polished part of the sample (to avoid overlapping with the platinum of the cup), fixed with adhesive tape, then coated with

gold. If a sample had been separated from its Pt cup, both sides of the sample would have to be coated. The samples were then loaded on their respective slots on a printed circuit board in a combinatorial cell equipped used to measure conductivity.[7] The cell was equipped with a polymer barrier around the printed circuit board to isolate the inner atmosphere argon from the outer one. To measure the ionic conductivity, an EIS measurement was taken from 1 MHz to 1 Hz with an amplitude of 100 mV.

The setup could then be heated to 50 °C, which allowed the activation energy to be calculated from the Arrhenius equation. Once cooled down, the electronic conductivity could then be measured by chronoamperometry, which applied a potential of 0.5 V, 1 V, 1.5 V, 2 V and 2.5 V, letting the current drop to a constant value over 1 h. An average of the current at steady state was then taken and the conductivity was calculated through Ohm's law.

After measuring the conductivity, the samples were then exposed to air (relative humidity of about 40%) and had their gold contact sanded off. They were then taken out of the Pt cups and ground up to characterize by powder X-ray diffraction (PXRD) in a high-throughput setup. A Panalytical Empyrean diffractometer with a Mo source (60 kV, 40 mA) and GalaPIX area detector were used to collect the XRD patterns in transmission mode. All the scans were done in the 4–30° scattering angle range of Mo Kα radiation (λ = 0.70926 Å for Kα1), which is approximately equal to the 10–70° angle range for Cu radiation. The XRD patterns were identified and refined using Panalytical's HighScore Plus software and multiple-phase Rietveld refinement was then performed on all XRD patterns where phase quantification was done.

3. Results and discussion

3.1 Overcoming elemental loss during melting

One of the established syntheses from the literature for these boracites is to first perform the melt-quench between 1000 °C and 1150 °C (depending on the B/M ratio) and then recrystallizing at a lower temperature (500–600 °C).[18] Fig. 2(a) shows the XRD pattern from a combinatorial sample (weighing roughly 80 mg only) made by this method. The pattern indexes perfectly to LiB_5O_8 even though the dispensing was made at the target composition of $Li_4B_7O_{12}Cl$. This suggests that both Li and Cl loss is a major concern at these conditions, and this is exacerbated by the high surface area to volume ratios in our combinatorial samples. Table 1 further shows the elemental analysis obtained from this sample using XPS both on the top of the sample and on the bottom surface after removing the sample from the Pt cup. It should be noted that the lithium content determined from XPS is approximative. The results show that all the Cl is gone from the surface, and the vast majority of it has also been removed from the bottom. Clearly, the Cl loss is extreme in these materials, and this proved to be the major obstacle to preparing these materials on the combinatorial scale. Fig. 2(a) shows various XRD patterns obtained during the optimization process. First, we tried to reduce the temperature, however, 950 °C proved to be the lowest temperature that permitted adequate melting of the samples. Even at 950 °C, the sample melting on its own (sample C) showed a high degree of oxide in the XRD pattern again showing severe Cl loss. By contrast, a material made at the same composition (D) with 63 other samples also in the furnace showed a pure boracite XRD pattern indexing to the target phase. This indicates that it is possible to saturate the box furnace with chlorine vapour such that equilibrium between the samples and the atmosphere can be established and thereby maintain a high Cl content. Fig. 2(b) shows the phase diagram where 64 samples are made at once and this effect can be clearly seen in the batch of samples made at the high Cl amounts (low Li/Cl ratio). In fact, to obtain the pure target boracite, we needed to dispense roughly 8× the amount of Cl needed in the target material. To our knowledge, this is the first time that atmospheric saturation is successfully utilized to make combinatorial samples that suffer elemental loss during high-temperature synthesis. It should also be emphasized that this approach can only be used when all target materials contain a comparable amount of chlorine, in this case 1 per formula unit; it would be exceedingly difficult to screen samples across Cl contents in this manner.

Table 1 Composition of melt-quenched samples as obtained by XPS. At 1150 °C, the dopant M was Al, for the other samples it was Ga. The terms "covered" and "uncovered" refer to whether an alumina boat was inverted and placed above the samples during the high temperature melting, the temperature refers to the melt temperature, and top/bottom refers to what side of the pellet was studied by XPS. It should be noted that the lithium content is approximative

Element	Target $Li_4B_7O_{12}Cl$	Covered 950 °C	Covered 1000 °C	Uncovered 1150 °C, top	Uncovered 1150 °C, bottom
Li	33.33%	36.78%	35.85%	22.51%	33.61%
B	58.33%	29.08%	47.65%	43.09%	34.79%
M	—	16.96%	12.72%	34.39%	31.26%
Cl	8.33%	17.18%	3.77%	~0%	0.31%

Upon identifying the saturated atmosphere as the means to successfully make these materials, we converted our melt-quench approach to simply melt 8 materials at once under an inverted alumina boat as shown in Fig. 1, and then to melt materials individually under smaller alumina cups. This method was successful at both 950 and 1000 °C as shown in the XRD patterns. Table 1 shows that both these materials also maintained much better Cl contents with the lower temperature giving a slight Cl excess while the higher temperature yields slight Cl deficiencies (at the top surface). Both XRD patterns show the successful synthesis of the boracite material, though the sample at 950 °C shows some $LiGa_5O_8$ phase, showing that Ga may saturate below the x = 3 content at this temperature (this is explored further in the next section). Overall, the fact that the sample from 950 °C shows a strong boracite XRD content and a high Cl content make them of high interest to characterize further, particularly for ionic conductivity.

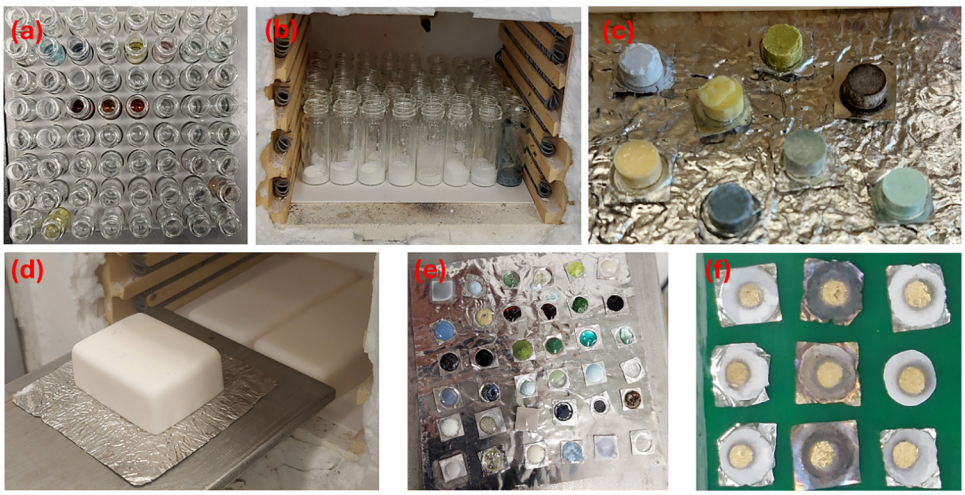

Fig. 1 Images showing the key steps in the final high-throughput synthesis workflow developed herein. First, solution mixtures are dispensed into vials (a), then the dried materials are heated in a box furnace to burn off all counter ions and byproducts (b). Samples are then pelletized and placed on platinum plates formed into shallow cups (c) and melt-quenching is performed under an alumina boat with 8 samples inside (d). The glassy materials (e) are then recrystallized, and a gold contact is sputtered on top to enable the conductivity measurements (f). The elements doped into each glassy material in (e) are labelled in Fig. 5(a).

3.2 Properties of optimal combinatorial material

We utilized our high-throughput experimental workflow to determine a number of important properties for solid electrolytes.[7] First, we performed EIS at both room temperature and 50 °C for a series of samples made with various Ga content. These samples were melted at 950 °C and melted well up to a Ga content of 2. Before crystallizing, these samples had a deformability of around 70 $mm^2\ kg^{-1}$ at 500 °C. The EIS spectra were fit using the typical equivalent circuit as discussed in ref. 7 to extract ionic conductivity. The results show an optimum Ga content where conductivities above 10^{-5} S cm^{-1} are obtained at 50 °C and about half that at room temperature. Heating the same precursor material (x = 2) at 1000 °C yields a completely glassy material after the melt-quench. It has a deformability of around 300 $mm^2\ kg^{-1}$ at 500 °C. After annealing and crystallizing, these samples have a total conductivity of around 3×10^{-6} S cm^{-1}. These values are largely consistent with those from ref. 18. The reported ionic conductivity for this material ($x = 2$) after melting at 950 °C is almost 10^{-5} S cm^{-1} (8×10^{-6} S cm^{-1} bulk conductivity and 5×10^{-6} S cm^{-1} total conductivity for $Li_4B_4Al_3O_{12}Cl$ and similarly for $Li_4B_4Ga_3O_{12}Cl$). The aluminum doped boracite in this work did not yield any measurable conductivity. The sample also has an electronic conductivity of 1.5×10^{-8} S cm^{-1}, which is two orders of magnitude lower than the ionic conductivity. The XRD pattern of the working sample herein shows a large amount $LiGa_5O_8$ and $Li_4B_7O_{12}Cl$, while the sample melted at

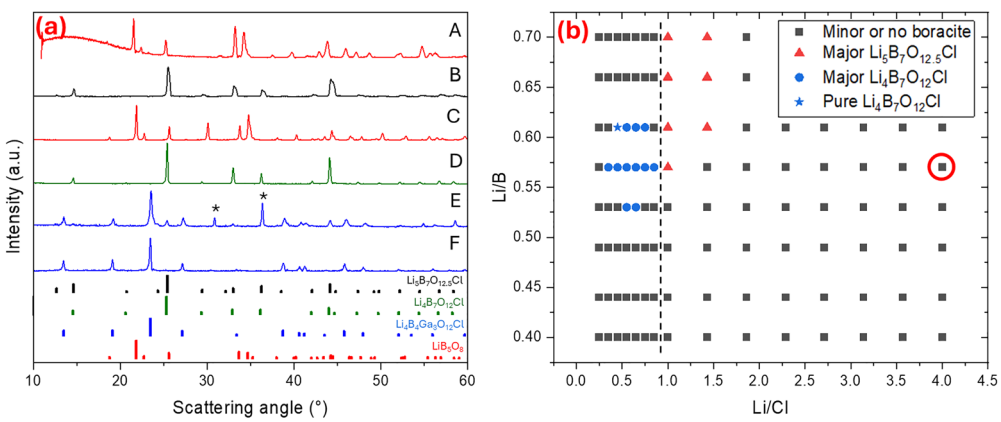

Fig. 2 (a) Powder XRD patterns (post-crystallization) of an aluminum-doped sample melted at 1150 °C for 30 minutes without cover (A), an undoped, unmelted boracite sample after sintering at 700 °C (B), an undoped sample melted at 950 °C without cover melted by itself in the furnace (C), an undoped sample melted at 950 °C without cover melted with 63 other samples in the furnace (D), a Ga-doped (x = 2) sample melted at 950 °C with 7 other similar samples under a small boat (E), a Ga-doped (x = 2) sample melted at 1000 °C by itself under a singular small crucible (F). (b) The phase diagram obtained with two batches of samples (separated by the dashed line) where each composition is the dispensed composition. The red circle indicates the target composition $Li_4B_7O_{12}Cl$. All samples in the phase diagram on one side of the dashed line were melt-quenched together from 950 °C without covering the samples in the furnace.

1000 °C has a near pure-boracite diffraction like those from ref. 18. The activation energy of 0.33 eV found in this work is in reasonable agreement with the reported value of 0.38 eV, though slightly lower.

Beyond conductivities, we also evaluate the electrochemical stability window by crushing the samples after conductivity measurements and performing a CV with the electrolyte being used as the electrode in a composite with conductive carbon and binder (this has been well established as the accurate way to determine stability window in ref. 6). Fig. 3(d) shows the resulting CV curves in comparison to a blank with conductive carbon and binder only. The results show that at high voltage (note: a different cell is used for high and low voltage) the boracite begins to react at about 4.3 V where its signal begins to exceed the blank. This means that the boracites are certainly perfectly stable with $LiFePO_4$, but that some limits on the upper voltage may be required in cells with layered oxide cathodes that often operate to 4.3 V *vs.* Li. On the low voltage side, the pristine material is stable all the way down to 0.15 V *vs.* Li (except at very low voltages where Li plating is likely). However, the aged sample that sat on the lab bench for a day at roughly 30% RH clearly shows that reduction begins above 2 V. This is the first indication that this material may in fact be unstable in air. This peak in fact matches exactly a peak seen in a sample to which we intentionally added a drop of liquid water (labelled added water) prior to drying the electrolyte for the stability window test. This establishes this peak near 2 V as a clear indicator of moisture instability and will serve as a useful metric in future high-throughput studies to identify dopants that might suppress this peak.

To further explore the air stability issue, we performed EIS on samples after various exposure times to the laboratory atmosphere (roughly 30% RH). Fig. 4 shows that the ionic conductivity increases dramatically in these materials after exposure to humid air, one can even see droplets forming on the surface of some materials as shown in the image. Fig. 4(a) shows the change in an undoped material and it is extreme: the conductivity reaches more than 1 mS cm^{-1} after air exposure and then decreases after drying at 50 °C. This is very much consistent with instability with water such that the high conductivity after air exposure is attributed to the material becoming a proton conductor. Similarly, Fig. 4(b) and (c) show the same effect in a Ga-containing sample where various air exposures increase the ionic conductivity by a factor of about 30, though drying at 50 °C shows no healing here, suggesting that more aggressive drying is needed (this is also the case for Fig. 4(a) where return to the pristine conductivity is not achieved).

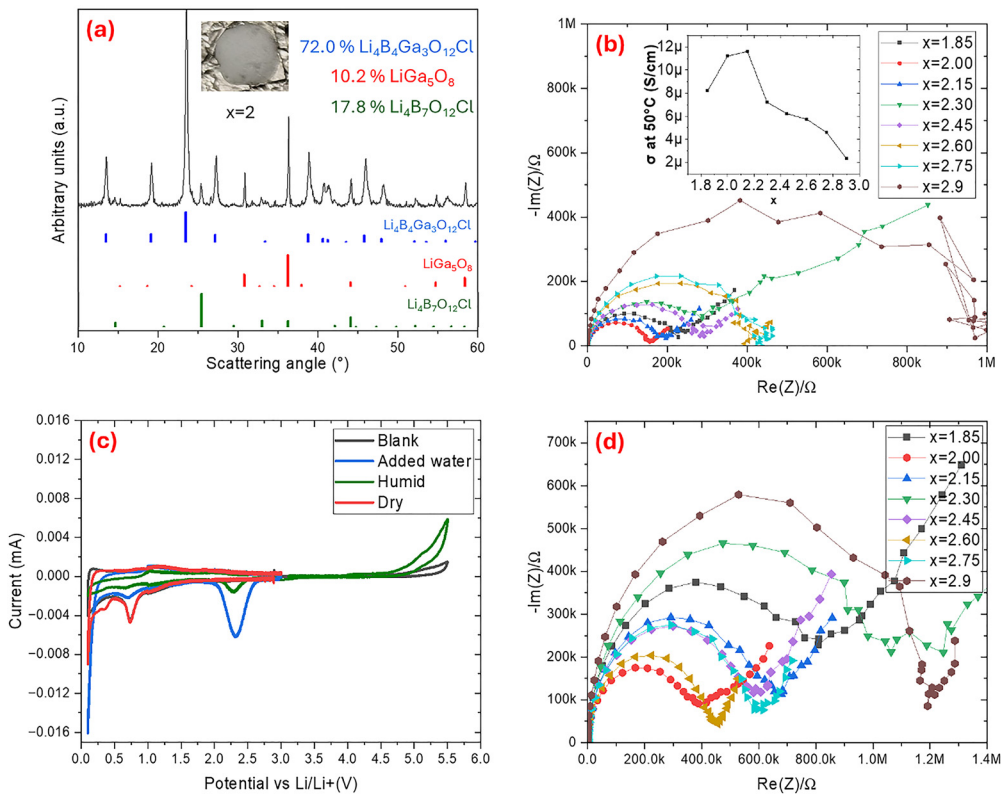

Fig. 3 Characteristics of gallium-doped samples melted at 950 °C, then crystallized at 525 °C for 3 hours. (a) A powder XRD pattern of a sample with a Ga content of $x = 2$, (b) the Nyquist plots and calculated conductivity (inset plot) at 50 °C for multiple x values, (c) cyclic voltammetry of a Li|LP30|carbon black/PVDF cells compared to that of Li|LP30|LiBGaOCl/carbon black/PVDF ($x = 2$) cells with samples exposed to humid air, dry samples, and sample with water added (a separate cell for high and low voltage was employed for the humid and blank sample) the blank overlaps with the dry sample at between 0.5 V and 3 V and (d) the Nyquist plots at room temperature for multiple x values.

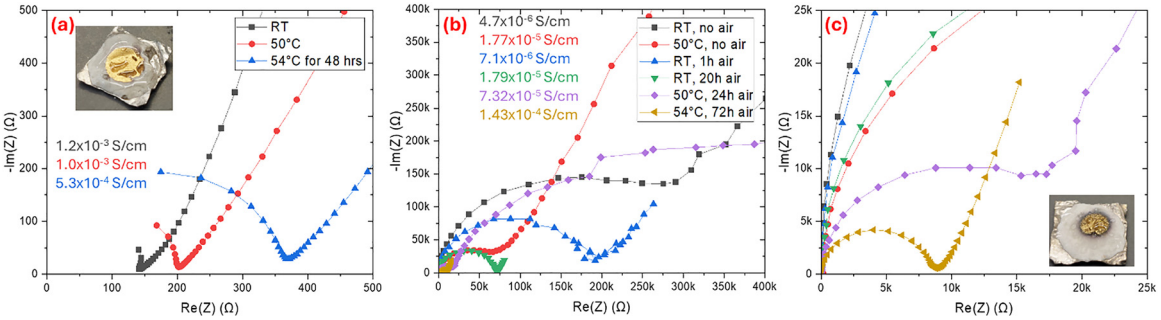

Fig. 4 (a) The effect of exposure to higher temperatures on an undoped ($Li_4B_7O_{12}Cl$) sample after over a day of air exposure (its conductivity before exposure was not measurable in our system indicating it was below 10^{-7} S cm^{-1}). (b) and (c) EIS spectra from a sample after various stages of air exposure. In all panels, the inset values are the ionic conductivities.

3.3 Prospects for high-throughput screening

As a proof of concept that the established combinatorial workflow can yield materials across wide compositions and tunable properties, we prepared a set of $Li_4B_6MO_{12}Cl$ with M being a list of 62 elements shown in Fig. 5(a). The materials in the image are after the melt-quenching step and they show a wide variety of sample structures with several of them showing well-melted materials highlighted in the periodic table in Fig. 5(b). We then performed dimple tests on the materials at 500 °C (a typical temperature used to process solid electrolytes with cathode materials). Whereas the undoped showed no dimple whatsoever, we find that quite a few of the substituted materials show very high deformability (1/BHN values of about 100 mm^2 kg^{-1} correspond to the consistent of a soft putty as discussed in ref. 8). This clearly shows the dramatic impact that dopants can have on the hardness of the boracites and is highly encouraging for future work. There are some interesting trends here that warrant some discussion. First, within the 3d metals, we find that as we go along the row the materials alternate between high and low deformability and this matches perfectly with whether or not they form pure glasses after quenching. The result is that Cr (non-deformable and not a pure glass) is surrounded by high deformability materials. We intend to follow-up on this in future work by lowering the doping levels to determine whether it is solely due to whether or not a glass is formed or if the dopant itself plays other roles in controlling deformability. Furthermore, in our previous work on the borosilicate glasses, we found that much lower substitution levels on the order of 2 at% are sufficient to dramatically alter the glass transition temperature (and thus the hardness) of the glass at the processing temperatures discussed in the introduction. It is also interesting that numerous samples show dramatic color change suggesting a transition to mixed conduction making them unsuitable as an electrolyte but they could be highly useful as dual conductor in the composite cathode. Our future work therefore aims to systematically screen this wide list of dopants at much lower substitution levels and determine the impact on all key properties including deformability, ionic/electronic conductivity, electrochemical stability, and air stability. The methods developed herein allow for the determination of all these properties in an efficient combinatorial workflow.

It is also worth noting that the significant air instability of these materials has not been reported previously and it illustrates that great care must be taken in handling these samples

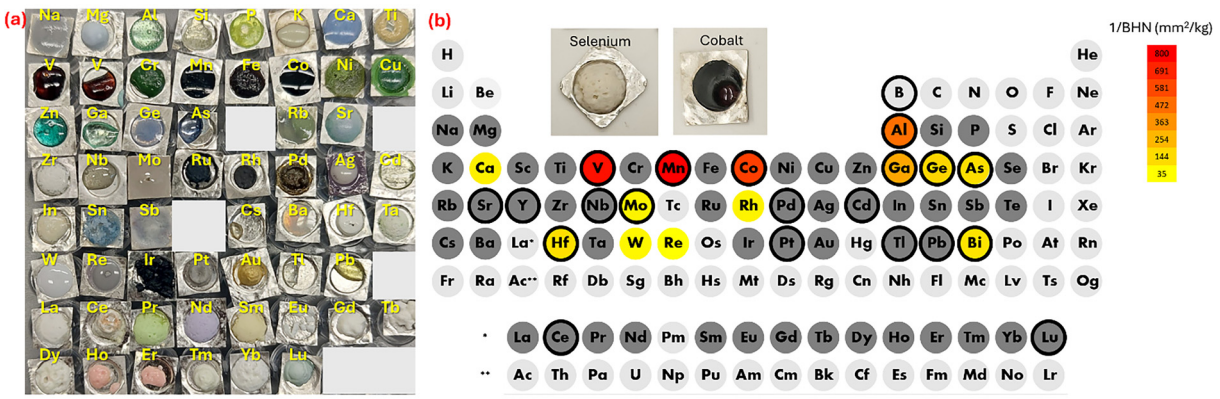

Fig. 5 (a) An image of the $Li_4B_6MO_{12}Cl$ samples after melt-quenching from 950 °C (this is uncovered, thereby matching the method from Fig. 2(b) where multiple samples are used to saturate the furnace with Cl). (b) Periodic table representing every dopant M used in the $Li_4B_6MO_{12}Cl$ formula with colors between yellow and red representing the deformability according to the scale on the right. Dark grey dopants were tried but were not deformable. The dopants whose sample was amorphous before crystallizing are circled in black.

and that exposure to humid air must be minimized. Our high-throughput workflow established herein is therefore to transfer the samples into an argon-filled glovebox after recrystallizing and gold coating is performed inside the glovebox. This eliminates the risk of drastically overestimating the ionic conductivity by inadvertently converting the material to a proton conductor. It is also important to reiterate that the reduction peak in the CV seen at 2 V *vs.* Li (Fig. 3(d)) in the material exposed to air will potentially serve as a useful screening to make sure that the materials have not been excessively exposed to air during the combinatorial workflow (the stability window is the last test performed). Alternatively, intentionally exposing the samples to air and then performing the stability window test will directly screen for materials that improve the air stability.

4. Conclusion

Boracites, such as $Li_4B_{7-x}Ga_xO_{12}Cl$, are an interesting class of potential solid electrolytes for lithium batteries as they combine deformability during cell assembly and rigidity during battery use. However, they remain very understudied with only a few compositions of Ga, Al and Mg doped materials having been published to date. Herein, we develop a combinatorial synthesis route which overcomes the extreme Cl loss during the high temperature melting by saturating the atmosphere with Cl and thereby reaching an equilibrium state in which the samples maintain the desired Cl content. Our characterization of the resulting materials shows comparable ionic conductivity to those reported previously and we further explore the deformability and the stability window of these materials for the first time. We find a wide electrochemical stability window (0.15 V up to 4.3 V *vs.* Li) showing promise in practical battery designs. We further demonstrate for the first time that these materials suffer from poor air stability with a reduction peak appearing at above 2 V *vs.* Li when the samples are exposed to air. Most alarmingly, the ionic conductivities of the materials can increase to above 1 mS cm^{-1}, but this is due to conversion to a proton conductor and not to improved Li transport. We therefore identify the storage conditions under which these materials must be maintained to give meaningful results. Finally, we demonstrate the viability of the high-throughput by systematically screening the impact of 62 different dopants on the deformability of the material after melt-quenching and find that this property is highly tunable. This motivates follow-up work using the high-throughput approach to develop viable electrolytes at much lower substitution levels.

Conflicts of interest

There are no conflicts to declare.

Data availability

Data for this article, including XRD, EIS and cyclic voltammetry are available on the Zenodo repository at the following DOI: **https://doi.org/10.5281/zenodo.15807860**.

Acknowledgements

This work was funded by the Natural Sciences and Engineering Research Council of Canada under the auspices of a Discovery grant and a research contract with industrial partner Samsung. JDL acknowledges the receipt of two NSERC graduate scholarships (CGS-M and PGS-D).

References

1 B. Diouf and R. Pode, Potential of Lithium-Ion Batteries in Renewable Energy, *Renewable Energy*, 2015, **76**, 375–380, DOI: **10.1016/j.renene.2014.11.058**.
2 L. Song, Y. Zheng, Z. Xiao, C. Wang and T. Long, Review on Thermal Runaway of Lithium-Ion Batteries for Electric Vehicles, *J. Electron. Mater.*, 2022, **51**(1), 30–46, DOI: **10.1007/s11664-021-09281-0**.
3 B. Li, Y. Chao, M. Li, Y. Xiao, R. Li, K. Yang, X. Cui, G. Xu, L. Li, C. Yang, Y. Yu, D. P. Wilkinson and J. Zhang, A Review of Solid Electrolyte Interphase (SEI) and Dendrite Formation in Lithium Batteries, *Electrochem. Energy Rev.*, 2023, **6**(1), 7, DOI: **10.1007/s41918-022-00147-5**.
4 Y. Takeda, O. Yamamoto and N. Imanishi, Lithium Dendrite Formation on a Lithium Metal Anode from Liquid, Polymer and Solid Electrolytes, *Electrochemistry*, 2016, **84**(4), 210–218, DOI: **10.5796/electrochemistry.84.210**.
5 Q. Lv, Y. Jiang, B. Wang, Y. Chen, F. Jin, B. Wu, H. Ren, N. Zhang, R. Xu, Y. Li, T. Zhang, Y. Zhou, D. Wang, H. Liu and S. Dou, Suppressing Lithium Dendrites within Inorganic Solid-State Electrolytes, *Cell Rep. Phys. Sci.*, 2022, **3**(1), 100706, DOI: **10.1016/j.xcrp.2021.100706**.
6 A. Jonderian and E. McCalla, The Role of Metal Substitutions in the Development of Li Batteries, Part II: Solid Electrolytes, *Mater. Adv.*, 2021, **2**(9), 2846–2875, DOI: **10.1039/D1MA00082A**.
7 A. Jonderian, E. Anderson, R. Peng, P. Xu, S. Jia, V. Cozea and E. McCalla, Suite of High-Throughput Experiments for Screening Solid Electrolytes for Li Batteries, *J. Electrochem. Soc.*, 2022, **169**(5), 050504.
8 A. Jonderian, S. Rehman, M. Card Gormley, S. Jia, S. B. Ma, G. Kwon and E. McCalla, Pioneering Combinatorial Investigation to Unlock the Potential of Lithium Borosilicate Glasses as Solid Electrolytes, *ACS Appl. Energy Mater.*, 2024, **7**, 11278, DOI: **10.1021/acsaem.3c02748**.
9 E. McCalla, Semiautomated Experiments to Accelerate the Design of Advanced Battery Materials: Combining Speed, Low Cost, and Adaptability, *ACS Eng. Au*, 2023, **3**(6), 391–402, DOI: **10.1021/acsengineeringau.3c00037**.
10 S. S. Gundale, V. V. Behare and A. V. Deshpande, Study of Electrical Conductivity of Li_2O–B_2O_3–SiO_2–Li_2SO_4 Glasses

and Glass-Ceramics, *Solid State Ionics*, 2016, **298**, 57–62, DOI: 10.1016/j.ssi.2016.11.002.

11 J. Zhou, P. Chen, W. Wang and X. Zhang, Li7P3S11 Electrolyte for All-Solid-State Lithium-Ion Batteries: Structure, Synthesis, and Applications, *Chem. Eng. J.*, 2022, **446**, 137041, DOI: 10.1016/j.cej.2022.137041.

12 X. Yu, J. Bates, G. Jellison and F. Hart, A Stable Thin-Film Lithium Electrolyte: Lithium Phosphorus Oxynitride, *J. Electrochem. Soc.*, 1997, **144**(2), 524–532, DOI: 10.1149/1.1837443.

13 B. Calès, A. Levasseur, C. Fouassier, J. M. Réau and P. Hagenmuller, Conductivite Ionique Du Lithium Dans Les Solutions Solides de Structure Boracite $Li_{4+x}B_7O_{12+x/2x}$, *Solid State Commun.*, 1977, **24**, 323.

14 T. Nagase, K. Sakane and H. Wada, Electrical Properties of Polycrystalline Lithium Chloroboracite Prepared by the Sol–Gel Method, *J. Sol-Gel Sci. Technol.*, 1998, **13**(1), 223–227, DOI: 10.1023/A:1008665119392.

15 N. I. Sorokin, Electrical Conductivity of Superionic Conductor Single Crystals $Li_4B_7O_{12}Cl_{1-x}Br_x$ ($x \sim 0.3$), *Phys. Solid State*, 2015, **57**, 314.

16 D. Tan, F. Wang, T. Pietsch, M. A. Grasser, T. Doert and M. Ruck, Low-Temperature Ionothermal Synthesis of Li-Ion Conductive $Li_4B_7O_{12}Cl$ Solid-State Electrolyte, *ACS Appl. Energy Mater.*, 2019, **2**(7), 5140–5145, DOI: 10.1021/acsaem.9b00812.

17 T. Katsumata, Y. Aoki, K. Fushimi, K. Otsuka, K. Ueda and Y. Inaguma, Synthesis and Ionic Conductivity of Li Boracites, $Li_4B_7O_{12}Cl$ and $Li_4B_4Al_3O_{12}Cl_{1-x}Br_x$, *Solid State Ionics*, 2022, **380**, 115921, DOI: 10.1016/j.ssi.2022.115921.

18 K. Kajihara, N. Tezuka, M. Shoji, J. Wakasugi, H. Munakata and K. Kanamura, $Li_4B_4M_3O_{12}Cl$ (M = Al, Ga): An Electrochemically Stable, Lithium-Ion-Conducting Cubic Boracite with Substituted Boron Sites, *Bull. Chem. Soc. Jpn.*, 2017, **90**(12), 1279–1286, DOI: 10.1246/bcsj.20170242.

19 M. Saito, H. Arima, M. Shoji, Y. Kizuki, H. Munakata, K. Kanamura and K. Kajihara, Solid-State Rechargeable Lithium Metal Battery with $Li_4B_4Al_3O_{12}Cl$-Based Water-Resistant Lithium-Ion-Conducting Oxychloride Glass-Ceramic Electrolyte, *J. Electrochem. Soc.*, 2021, **168**(4), 040524, DOI: 10.1149/1945-7111/abf4b0.

20 S. Wang, Z. Gao, F. Sun, Y. Yang, L. Tao, Y. Wang, Z. Yu, J. Wu, J. Hou, Z. Liu, H. Song and H. Chen, Li Vacancy-Induced Ionic Conductivity Enhancement in $Li_4B_7O_{12}Cl$ for All-Solid-State Li-Ion Battery Application, *New J. Chem.*, 2024, **48**(27), 12199–12208, DOI: 10.1039/D4NJ00414K.